

Journal of Materials Chemistry B

Accepted Manuscript



This is an *Accepted Manuscript*, which has been through the Royal Society of Chemistry peer review process and has been accepted for publication.

Accepted Manuscripts are published online shortly after acceptance, before technical editing, formatting and proof reading. Using this free service, authors can make their results available to the community, in citable form, before we publish the edited article. We will replace this *Accepted Manuscript* with the edited and formatted *Advance Article* as soon as it is available.

You can find more information about *Accepted Manuscripts* in the [Information for Authors](#).

Please note that technical editing may introduce minor changes to the text and/or graphics, which may alter content. The journal's standard [Terms & Conditions](#) and the [Ethical guidelines](#) still apply. In no event shall the Royal Society of Chemistry be held responsible for any errors or omissions in this *Accepted Manuscript* or any consequences arising from the use of any information it contains.



Preparation of rhBMP-2 loaded mesoporous bioactive glasses/calcium phosphate cements porous composite scaffold for rapid bone tissue regeneration

Received 00th January 20xx,
Accepted 00th January 20xx

DOI: 10.1039/x0xx00000x

www.rsc.org/

Nan Li^{a,†}, Chuan Jiang^{b,†}, Xingdi Zhang^a, Xinfeng Gu^b, Jingwei Zhang^b, Yuan Yuan^a, Changsheng Liu^a, Jianlin Shi^c, Jinwu Wang^{b,*} and Yongsheng Li^{a,*}

In this work, a novel composite scaffold was conducted by combining mesoporous bioactive glasses (MBG) and calcium phosphate cements (CPC) materials with a simple centrifugal embedding approach. Furthermore, recombinant human bone morphogenetic protein-2 (rhBMP-2) was facily incorporated into this scaffold through a freeze-drying process. It is found that the resultant scaffold not only presents hierarchical pore structure (interconnected pores of around 200 μm and 2-10 μm) and sufficient compressive strength (up to 1.4 MPa), but also exhibits excellent drug delivery property, presenting sustained release of rhBMP-2 for over 7 d. In order to evaluate the osteogenetic capacity of rhBMP-2 loaded MBG/CPC scaffold, in vitro cell culture with bone marrow stromal cells (BMSCs) was conducted. Notably, this composite scaffold presents favorable effect to the proliferation and osteogenetic differentiation of BMSCs. Furthermore, in vivo bone tissue regeneration was conducted with a rabbit radius defect model. It is demonstrated that the incorporation of rhBMP-2 can induce significant improvement of osteogenetic efficiency, especially in the early stage. Moreover, better biodegradability was obtained in the rhBMP-2 loaded MBG/CPC scaffold than the others. Therefore, it is anticipated that the rhBMP-2 loaded MBG/CPC scaffold is of great potentials in the field of rapid bone tissue regeneration.

1. Introduction

Nowadays, bone defects caused by trauma, injury or resection of tumors have been clinically treated by the implantation of autogenous and allogeneous bone grafts. Although autogenous bone grafting is considered the current gold standard for reconstructive surgery, the shortage of donor supply and the risk of reoperation limit its applications. As for the allogeneous bone grafting, the risks of disease transmission and immunological rejection are problems to be resolved.¹⁻³ Alternative methods for bone defects repair, such as bone tissue engineering techniques, could bring new opportunities.⁴⁻⁸

Over the last few years, the development of synthetic scaffolds for applications in bone tissue regeneration represents a significant challenge to current regenerative medical research. It is known that, bone is mostly made up of a composite material incorporating the

inorganic mineral calcium phosphate and organic collagen, and interconnected macropore structure could give accessibility for guest molecules and cells going through the inorganic network via pores and channels. Therefore, porous Ca/P scaffolds of multiple length scales have attracted much attention. Porous calcium phosphate cements (CPC) scaffolds, having proven to be biocompatible, osteoconductive and injectable, are commonly used as bone-filling materials in the field of dentistry and orthopedic surgery.^{9,10} However, undesirable behavior of drug delivery and slow resorption in vivo, which are unfavorable to bone formation, make it less applicable for the purpose of tissue engineering.¹¹ The incorporation of bioactive materials into CPC is considered to be a promising method that can significantly alter the physic-chemical and biological properties. Consequently, several approaches have been explored to improve the osteogenetic properties of CPC by introducing bioactive polymers or nanomaterials.¹²⁻¹⁵

Mesoporous bioactive glasses (MBG), which possess high specific surface area, well ordered pore channels and large pore volume, have been addressed to be potential materials for bone tissue regeneration.¹⁶⁻¹⁸ Up to now, numerous types of porous MBG scaffolds have been successfully prepared, showing excellent bioactivity and drug release behaviors.¹⁹⁻²¹ Unfortunately, they are facing with a series of problems. Especially, low fracture strength and stiffness make it difficult for MBG scaffolds to be used in the clinic.^{22,23} In fact, some recent studies have confirmed that the incorporation of biocompatible inorganic nanoparticles into CPC materials could remarkably promote the bioactivity and biodegradability.²⁴⁻²⁸ In view of this, the combination of CPC and

^a Key Laboratory for Ultrafine Materials of Ministry of Education, East China University of Science and Technology, Shanghai 200237, China. E-mail: ysl@ecust.edu.cn; Fax: +86-21-64250900; Tel: +86-21-64250900

^b Shanghai Key Laboratory of Orthopedic Implant, Department of Orthopedic Surgery, Shanghai Ninth People's Hospital Affiliated Shanghai Jiao Tong University School of Medicine, Shanghai 200011, China. E-mail: jinwu_wang@163.com; Fax: +86-21-23271699; Tel: +86-21-23271699

^c State Key Lab of High Performance Ceramics and Superfine Microstructure, Shanghai Institute of Ceramics, Chinese Academy of Sciences, Shanghai 200050, China.

[†] Electronic Supplementary Information (ESI) available: See DOI: 10.1039/x0xx00000x

[‡] Co-first author: These authors contributed equally to this work.

MBG materials is expected to be a feasible approach to fabricate composite scaffolds with improved osteopromotive properties.

On the other hand, there is a general hypothesis that the primary contributors to acquire osteoinductivity consist of the formation of a biological apatite layer and the co-precipitation of endogenous osteoinductive proteins which stimulate the chemotaxis and differentiation of osteoprogenitor cells.²⁹ Bone morphogenic proteins (BMPs) are considered to be the most powerful osteogenetic growth factors.³⁰ Among them, recombinant human bone morphogenetic protein-2 (rhBMP-2) shows good effects in clinic applications, having been successfully used in the treatment of different animal models of bone defect since being approved by U.S. Food and Drug Administration and the European Medicines Agency in 2002.^{31,32} However, the rhBMP-2 administered in solution form does not always induce bone regeneration as much as expected because of the short-term retention of BMP activity in vivo. Therefore, how to achieve sustained release of growth factors in the defect areas over an extended time period is of great importance in tissue engineering. Up to now, delivering rhBMP-2 at a therapeutically effective dose, which could improve the utilization efficiency of rhBMP-2, remains still challenges in practical applications.

In this study, porous CPC scaffold with MBG powder filled in the framework has been successfully prepared. Following this, rhBMP-2 was incorporated into the as-prepared scaffold by freeze-drying process. In contrast to previous studies, where bioactive glasses or mesoporous silicate nanoparticles were used as the additives during the setting process¹¹⁻¹⁵, the current study is to introduce MBG, which possesses better bioactivity, into CPC materials via the post-synthesis process with a simple centrifugal embedding approach. The microstructure and compressive strength of the resultant MBG/CPC scaffold were firstly characterized. Then, rhBMP-2 loaded MBG/CPC scaffold was comprehensively investigated by in vitro cellular response using BMSCs as a cell-model and in vivo new bone formation using a rabbit radius defect model. To validate the beneficial effects of the composite scaffold, the relative cell proliferation was analyzed by SEM, confocal microscopy and CCK-8 assay. Additionally, alkaline phosphatase (ALP) activity, calcium deposition capability and osteogenetic gene expression were assayed to determine whether osteogenetic differentiation could take place. Furthermore, micro-CT evaluation, histological observations, biomechanical test and fluorescent double-labeling were employed to demonstrate the positive effect of rhBMP-2 loaded MBG/CPC scaffold on rapid bone tissue formation.

2. Materials and methods

2.1. Fabrication and characterization of CPC and MBG/CPC scaffolds

The MBG and CPC materials were prepared via the method reported before.^{16,33} In a typical synthesis of MBG/CPC scaffold, MBG (0.8 g) were dispersed into ethanol (30 mL) under continuous stirring for 15 min. The suspension obtained above was then transferred into a centrifuge tube of 50 mL, and the CPC scaffold was added. After being centrifuged with a speed of 7000 rpm/min for three times, the scaffold was taken out and washed with ethanol. Finally, the scaffold obtained above was dried at room temperature for 24 h under

vacuum. The content of MBG powder embedded into CPC scaffold was determined by the variation of weight for the scaffold before and after treatment.

The porosity of the scaffolds prepared above was measured by Archimedes' principle: $\Phi 10 \times 5$ mm sized scaffolds were used in the measurement and water was used as liquid medium. The porosity (P) was calculated according to the following formulation $P = (W_2 - W_1) / (W_2 - W_3) \times 100\%$, where W_1 is the dry weight of the scaffolds, W_2 is the weight of scaffolds saturated with water, and W_3 is the weight of scaffolds suspended in water.

The morphology and microstructure of the scaffolds were ascertained by X-ray diffraction (XRD, D8 Focus, Bruker, Ettlingen, Germany), scanning electron microscope (SEM, S-4800N, Hitachi, Tokyo, Japan) and Brunauer-Emmet-Teller (BET, Novawin 4200e, Quantachrome, Beijing, China).

2.2. Compressive strength and ion release of CPC and MBG/CPC scaffolds.

The compressive strength of $15 \times 5 \times 5$ mm sized scaffolds were tested using an Instron 5566 computer-controlled universal testing machine (Instron Wolpert, Darmstadt, Germany) at a crosshead speed of 0.5 mm/min.

The assessment of the ion release was carried out in a simulated body fluid (SBF) proposed by Kokubo et al.³⁴ The SBF solution has an ionic composition and concentration similar to those of the human plasma, prepared by dissolving NaCl, NaHCO₃, KCl, K₂HPO₄·3H₂O, MgCl₂·6H₂O, CaCl₂ and Na₂SO₄ into distilled water. The pH of the buffer solution was adjusted to 7.4 with (HOCH₂)₃CNH₂ and HCl.

The CPC and MBG/CPC scaffolds were soaked in the SBF solution with a mass/volume ratio of 2 mg/mL at a constant speed of 160 rpm/min under a constant temperature of 37 °C. After soaking for periods from 8 h to 3 d, the samples were removed and the supernatants were collected for the follow-up tests. The concentrations of released ions of calcium (Ca), silicon (Si), phosphorus (P) in the medium were examined by inductively coupled plasma optical emission spectrometry (ICP-OES, Agilent 710, Varian, Australia).

2.3. Loading and release of rhBMP-2

The CPC and MBG/CPC scaffolds were sterilized by Co₆₀- γ ray in advance. Then rhBMP-2 in acetic acid solution was blotted onto each sample in sterile conditions and stayed for 4 h to be totally absorbed. The dosage of rhBMP-2 within each scaffold was 1 μ g for cell culture and 20 μ g for implantation. Finally, the scaffolds were freeze dried for 24 h and stored at 20 °C for later use.

To investigate the in vitro release curve of rhBMP-2 from CPC and MBG/CPC scaffolds, each scaffold was put into a straight shaped glass bottle containing 2 mL SBF solution (pH=7.4). The bottle was incubated at 37 °C in a constant temperature incubator shaker at 100 rpm/min. Then, the total release medium was taken out at the pre-determined time intervals, and replaced with an equal amount of fresh SBF solution. This regimen was continued for 7 d, and the amount of released rhBMP-2 was measured using a BMP-2 ELISA kit (PeproTech, Rocky Hill, USA). The release curve was calculated in terms of the cumulative release percentage of rhBMP-2 (% , w/w) with incubation time.

2.4. Attachment and viability of BMSCs

Animals used in this experiment were all obtained from the Ninth People's Hospital Animal Center (Shanghai, China), and all animal procedures were approved by the Animal Experiment and Care Committee of Ninth People's Hospital affiliated to Shanghai Jiao Tong University School of Medicine. Rat bone marrow stromal cells, harvested from the tibia and femur of adult rats (4–6 weeks) and cultured according to the procedures described in a previous study, were used in the *in vitro* study. Cells from the third generation were used for further tests.³⁵

Φ10×5 mm sized CPC, MBG/CPC and rhBMP-2 loaded MBG/CPC scaffolds were placed in 24-well plates and incubated in Dulbecco's Modified Eagle Media (DMEM, Hyclone, Logan, UT, USA) overnight. The media were aspirated off and then 2×10⁴ BMSCs in a 200 μL suspension volume were placed on each scaffold. The cells were allowed to adhere to the scaffolds for 1 h before the scaffolds were covered with 1 mL of culture medium (DMEM+10% FBS).^{23,36}

(1) After 3 d of incubation, the scaffolds were washed with PBS twice and fixed with 4% paraformaldehyde (PFA) for 15 min. The morphological characteristics of the attached cells were observed using SEM (Quanta 250, FEI, Hillsboro, USA), and confocal laser scanning microscope (CLSM, Nikon, Tokyo, Japan) in which the cytoskeleton was stained with FITC-Phalloidin (Sigma-Aldrich, St. Louis, USA) and the nuclei were stained with DAPI (Sigma-Aldrich, St. Louis, MO, USA).

(2) After 3 and 7 d of incubation, a cell proliferation assay was performed using CCK-8 (Cell Counting Kit-8, Dojindo, Kumamoto, Japan) according to the manufacturer's instruction. The CCK-8 suspension cells were incubated for 2 h in 5% CO₂ at 37 °C. The proliferation of BMSCs on different scaffolds was evaluated by measuring the optical density (OD) level of the cells at 450 nm (630 nm as reference) using a microplate reader (Thermo, Minneapolis, USA).

2.5. Extractions of the scaffolds and their effects on BMSCs

The CPC, MBG/CPC, and rhBMP-2 loaded MBG/CPC scaffolds were placed in 10 mL tubes with 3 mL of DMEM medium, and incubated at 37 °C in a humidified atmosphere of 95% air and 5% CO₂. The extractions were collected and refreshed with DMEM every 3 d.³⁷ The collected extractions were supplemented with 10% fetal bovine serum (FBS) and osteogenesis induced ingredients (0.1 μM dexamethasone, 50 μg/mL ascorbic acid and 10 mM sodium β-glycerophosphate) for the following experiments.

2.5.1. Alkaline phosphatase (ALP) activity assay

A total of 5×10⁴ BMSCs were seeded into 24-well plates and induced into osteoblasts in the extractions mentioned above. After an incubation period of 7 and 14 d, the cells from each group were fixed for ALP staining and observed with the naked eye and optical microscope. For ALP quantitative assay, the cells were collected and detected according to the supplier's guideline (Nanjing Jiancheng Biotechnology Institute, Nanjing, China). The absorbance of ALP was measured by testing optical density (OD) values at 520 nm.

2.5.2. Calcium deposition assay

After 28 d of incubation, the cells from each group were fixed with 4% PFA, rinsed with PBS and stained with 40 mM Alizarin Red S for 20 min. Finally, the cells were washed thoroughly with PBS. The calcium deposits exhibited as red nodules on the cells surface and were observed with the naked eye and optical microscope.

2.5.3. Real time-polymerase chain reaction (PCR) analysis

The effect of different scaffolds on osteogenetic differentiation was further assessed by real time-PCR to measure the mRNA expression of ALP, runt-related transcription factor 2 (Runx 2), osteocalcin (OCN) and type I Collagen (COL I). 1×10⁵ BMSCs were seeded into 12-well plates, and total mRNA was isolated using the Qiagen kit (Valencia, CA, USA) according to the manufacturer's instructions after 14 d of induction culture. Subsequently, cDNA was synthesized from 1 μg of total RNA using Takara (Otsu, Japan), and real time-PCR was performed by Bio-Rad real-time PCR system (Bio-Rad, Hercules, USA). Primer sequences were as follows: ALP: forward, 5'-AGGGTGGGTTTCTCTCTTGG-3', and reverse, 5'-ACTGGCTGTGACTATGGGAC-3'; Runx2: forward, 5'-GGGACCGACACAGCCATATA-3', and reverse, 5'-GTCTCGGAGGGAAGGATGAG-3'; OCN: forward, 5'-CCTACAAGCGCATCTATGGC-3', and reverse, 5'-CTGTGCCGTCCATATTTTCG-3'; COL I: forward, 5'-TCCCTACCCTCAGCTTCTCT-3', and reverse, 5'-AGTCTCTTGCTTCCCTCCAC-3'; β-actin: forward, 5'-CACCATGTACCCAGGCATTG-3', and reverse, 5'-CACACAGAGTACTTGCCTC-3'. Relative expression levels for each gene were calculated and normalized against β-actin.

2.6. *In vivo* osteointegration evaluation

2.6.1. Animals

A total of 36 healthy male New Zealand rabbits, aged 6 months old, were used. According to the types of different scaffolds and time intervals, the rabbits were divided into six experimental groups, each of which concluded 6 rabbits.

2.6.2. Surgery procedures

15×5×5 mm sized CPC, MBG/CPC and rhBMP-2 loaded MBG/CPC scaffolds were used as implant materials. Anesthetic induction was obtained by intraperitoneal injection of 20% 10 mL/kg ketamine HCl. After shaving and disinfection in the mid-shaft of rabbit radius, the radius was exposed through a longitudinal incision of the skin. Then a defect of around 5 mm diameter and 15 mm height was made on the mid-shaft of radius for scaffold implantation. It is necessary to add that, the left radius of a rabbit was used for scaffold implantation, while the right radius was chosen at random as defect group or normal group. The surgical wound was closed carefully.

2.6.3. Fluorescent labeling

The bone formation rate was estimated using a fluorescent double-labeling method. Calcein (20 mg/kg) and Alizarin Red S (30 mg/kg) were administered intraperitoneally in turn at 5, 7, 13 and 15 w after the surgery procedures.

2.6.4. Sample preparation

After healing, for 8 and 16 w, the animals were sacrificed with an overdose of KCl solution. The radii including different scaffolds were harvested and trimmed into smaller ones. All specimens were fixed in 4% PFA immediately for subsequent experiments.

2.6.5. Biomechanical tests

To evaluate the repairing effect on the defect sites, the compressive strength of different specimens (including the normal group as control) harvested at different time nodes were tested by using an Instron 5566 computer-controlled universal testing machine. Briefly, the specimens whose length were 20 mm were dried under vacuum environment at 37 °C in advance, then both ends of bones were burnished using abrasive paper so that smooth surface could be obtained, which was essential to make the experiment data more reliable. The crosshead speed was set as 1 mm/min and the data generated in the test were automatically recorded.

2.6.6. Micro-CT analysis

All specimens were scanned for bone formation within the defects after implant retrieval with a μ CT imaging system (Instron, High Wycombe, UK) with the resolution of 18 μ m. After scanning, three-dimensional (3D) images were reconstructed and observed using GEHC MicroView software (GE Healthcare BioSciences, Chalfont St. Giles, UK).

2.6.7. Hematoxylin and Eosin (H&E) staining

After being fixed with 4% PFA, the radii containing different scaffolds were decalcified in 10% EDTA. Finally they were embedded in paraffin, and sectioned at a thickness of 5 μ m. For histological analysis, the sections were deparaffinized, and stained with hematoxylin and eosin. The sections were examined under a light microscope (DM 2500, Leica, Solms, Germany) connected to a personal computer.

2.6.8. Hard tissue slicing

After being fixed with 4% PFA, the radii containing different scaffolds were dehydrated with a graded series of alcohol, and embedded in polymethylmethacrylate (PMMA). The samples were cut into 150–200 μ m thick sections perpendicular to the scaffolds under cooling water with a sawing microtome. The sections were then glued onto a plastic support and polished to 50 ± 10 μ m in thickness. Fluorescence double-labeling observation was carried out under confocal laser scanning microscope. Excitation/emission wavelengths of chelating fluorochrome were used 488/525 and 561/595 nm for Calcein (green) and Alizarin Red S (red), respectively. Then, the slides were stained with Van Gieson's picrofuchsin staining. The assessment of the quantity of newly formed bone was obtained via the image analysis software (Image Pro Plus 6.0).

2.7. Statistical analysis

The data were presented as mean \pm standard deviation. Statistical analysis was performed with one-way analysis of variance (ANOVA). A value of $p < 0.05$ was considered statistically significant.

3. Results and discussion

3.1. Characterization of the composite MBG/CPC scaffold

3.1.1. Microstructure and morphology

Wide angle XRD patterns for CPC, MBG and MBG/CPC powder are shown in Fig. 1A. It can be seen that the diffraction pattern of MBG exhibits a broad peak for amorphous SiO_2 , while that of CPC presents the diffraction peaks of traditional hydroxyapatite (HA) (25.9° , 31.8° , 32.1° , 32.9° , 39.2° , 46.6° , 49.4° and 53.2°). For MBG/CPC powder, characteristic peaks of both CPC and MBG are detected, confirming the successful combination of MBG and CPC materials.

Fig. 1B presents the N_2 adsorption-desorption isotherms of MBG powder, CPC scaffold and MBG/CPC scaffold. The curve of MBG powder can be identified as type IV isotherm with a H1 hysteresis loop, typical for mesoporous materials with a narrow pore size distribution centered at 5.3 nm. For the CPC scaffold, the isotherm demonstrates a macroporous structure. Interestingly, a small hysteresis loop appears in the relative pressure range of 0.4 to 0.6 for the MBG/CPC scaffold, suggesting the existence of MBG powder and its incorporation in the framework of the CPC scaffold. The specific surface areas of MBG powder, CPC scaffold and MBG/CPC scaffold were calculated to be 364, 13.8 and 29 m^2/g , respectively. SEM images of CPC scaffold with different magnifications are presented in Fig. 1C (C1 & C2). As shown, macropores with size of around 200 μ m, and 2–10 μ m, which may be attributed to the recrystallization and leaching of the NaCl granules in the process of solidation, are distributed onto the scaffolds. Fig. 1C3 shows the SEM image of the cross section of the MBG/CPC scaffold. Some irregular shaped particles, in accordance with the morphology of MBG powder (data not shown), can be observed set into the macropores mentioned above. These further confirm the hierarchical pore architecture of MBG/CPC scaffold and the successful incorporation of MBG. Besides, the embedding amount of MBG powder into CPC scaffold is about 15 to 20 wt%, and the porosities of the open pores are estimated to be over 70% for both CPC and MBG/CPC scaffolds.

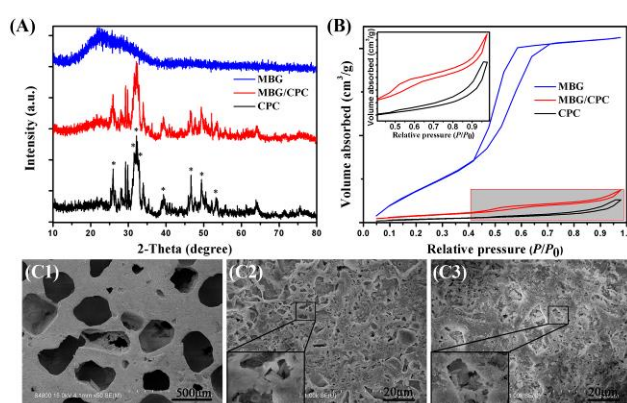


Fig. 1 (A) Wide angle XRD patterns for CPC, MBG and MBG/CPC materials (* for peaks of HA). (B) N_2 adsorption-desorption isotherms for MBG powder, CPC scaffold and MBG/CPC scaffold. (C) SEM images of CPC scaffold (C1, the images were taken at 50 \times magnification; C2, 1000 \times) and MBG/CPC scaffold (C3, 1000 \times). The insert images were taken at 10k \times magnification.

3.1.2. Compressive strength

Fig. 2 presents the compressive strength of the different scaffolds. The maximum load for MBG/CPC scaffold was measured to be 1.45 ± 0.12 MPa, similar to that of the CPC scaffold, 1.51 ± 0.19 MPa. This shows that the incorporation of MBG powder did not influence the inherent compressive strength of CPC scaffold.

Considering that porosity plays an important role in aiding cell functions and providing a favorable environment for cellular infiltration and nutrient transportation, and the compressive strength is also an important parameter for the implanted scaffolds for bone regeneration, it is believed that the as-synthesized MBG/CPC scaffold is an ideal implanting material for further study.

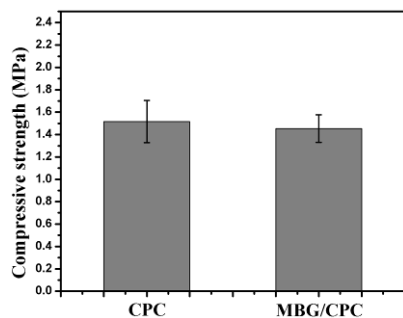


Fig. 2 Compressive strength of different scaffolds.

3.2. Ion release from various scaffolds and the releasing character of rhBMP-2

Cumulative release profiles of different ions in SBF are shown in Fig. 3A. As can be seen, the concentration of Ca^{2+} released from MBG/CPC scaffold reaches a maximum of 96 ppm at 8 h, and then experiences a quick decrease. In comparison, Ca^{2+} from the CPC scaffold decreases continuously during the whole testing period. The concentration curves of PO_4^{3-} released from both CPC and MBG/CPC scaffolds present the similar trends, gradually decreasing with the testing durations. In addition, the release of SiO_4^{4-} was detected for MBG/CPC scaffold. After a fast release in 24 h, the concentration of SiO_4^{4-} starts to reach constant. As the dissolution of Si and Ca species is beneficial to the formation of nucleation sites, it is expected that the MBG/CPC scaffold might exhibit better performance than CPC scaffold in the subsequent deposition of bone-like hydroxyapatite.

Fig. 3B reveals the releasing curves of rhBMP-2 loaded CPC and MBG/CPC scaffolds. It is found that both of the release curves can be divided into two stages: an initial fast releasing period followed by a slow one. However, the MBG/CPC scaffold presents a slower releasing rate of rhBMP-2 than that of CPC scaffold. Based on the results shown in Fig. 3B, it was calculated that around 52% of rhBMP-2 was released in the first 24 h from MBG/CPC scaffold, and the rest was released in a slower rate over a 144 h period. In contrast, about 68% rhBMP-2 was released in the first 24 h for CPC scaffold. These imply that the rhBMP-2 loaded MBG/CPC scaffold presents a slower and more sustained release behavior over the entire testing period, in comparison to that of the CPC scaffold. This might be attributed to the fast formation of HCA layer for MBG/CPC scaffold, and thus hinder the dissolving out of rhBMP-2.³⁸⁻⁴¹ Based

on this fact, the rhBMP-2 loaded CPC scaffold was not investigated any more in the following parts.

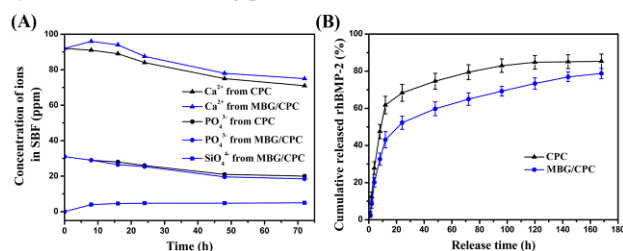


Fig. 3 (A) Ion release curves and (B) releasing performance of rhBMP-2 from CPC and MBG/CPC scaffolds.

3.3. Cell attachment, morphology and viability

The attaching performance and morphology of BMSCs on the CPC, MBG/CPC and rhBMP-2 loaded MBG/CPC scaffolds were examined by SEM and CLSM techniques. After 3 d of culture, BMSCs were found to attach onto the surface of all scaffolds. There is no distinct difference in the cell morphology or structure among the BMSCs attaching onto the three types of scaffolds (Fig. 4A & B). The cell proliferation results obtained by the CCK-8 assay are shown in Fig. 4C. After 3 or 7 d of culture, all the three scaffolds exhibit high viability of cells, demonstrating that each of them is capable to support the proliferation of BMSCs.

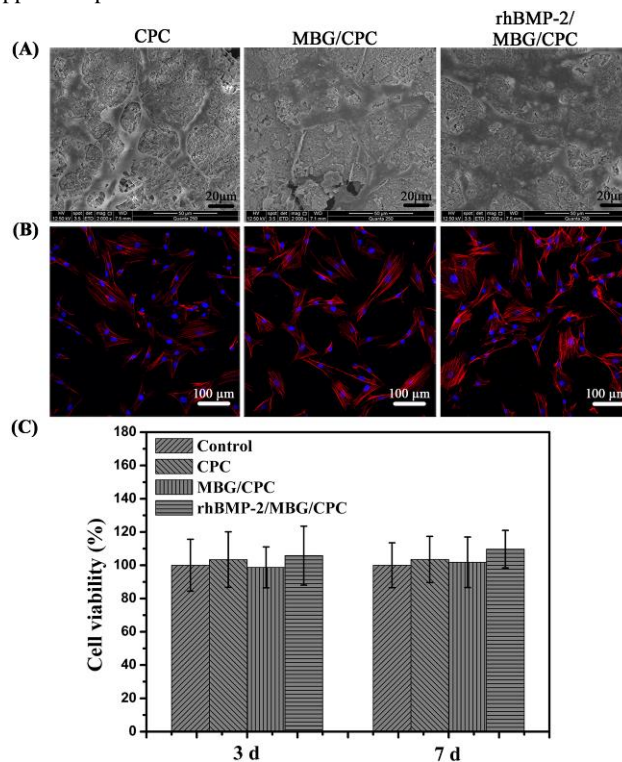


Fig. 4 Cell morphology and viability of BMSCs on CPC, MBG/CPC and rhBMP-2 loaded MBG/CPC scaffolds. (A) SEM images of BMSCs attachment and morphology after 3 d of culture. (B) CLSM images of cytoskeleton stained with FITC-Phalloidin (red) and nuclei stained with DAPI (blue) of BMSCs. (C) Proliferation of BMSCs on different scaffolds during culture for 3 and 7 d by CCK-8 assay.

3.4. Effects of dissolved components from scaffolds on BMSCs

To understand the influence of the dissolved components from different implanting scaffolds, ALP activity and calcium deposition capability were used as early markers to detect the BMSCs differentiation behavior. As shown in Fig. S1A (ESI[†]), after 7 d of incubation, the ALP-positive area for rhBMP-2 loaded MBG/CPC scaffold is larger than that for the others, and this trend becomes distinct with the incubation period extended to 14 d. Fig. S1B (ESI[†]) presents the corresponding areas of bone nodules formation measured by Alizarin Red S staining. Similarly, the rhBMP-2 loaded MBG/CPC scaffold shows the largest area, demonstrating its excellent mineralization capability. Notably, almost no difference is found among the CPC scaffold, the MBG/CPC scaffold and the control group in ALP-positive or mineralization areas, confirming that the osteoinductivity of scaffolds without rhBMP-2 is not enough to accelerate the osteogenetic differentiation of BMSCs.

Furthermore, quantitative analysis on the ALP activity was conducted and the results are shown in Fig. 5A. The ALP activities of cells in the extractions from CPC and MBG/CPC scaffolds are similar to that of the control group after 14 d of culture. However, the rhBMP-2 loaded MBG/CPC scaffold exhibits a significantly higher value. Moreover, the osteogenetic marker genes, ALP, Runx2, OCN and COL I were assessed by RT-PCR (Fig. 5B, C, D, E). Similar to the above results, the gene expression gets significantly enhanced in BMSCs cultured in rhBMP-2 loaded MBG/CPC scaffold, and the numerical values for the other groups show little difference between each other. Therefore, it is anticipated that the incorporation of rhBMP-2 into the implanting scaffolds is of great importance to the repair of bone segment defects.

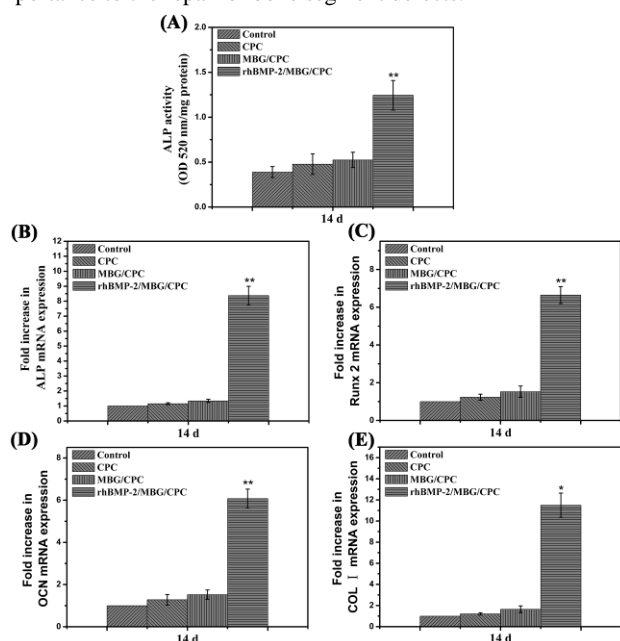


Fig. 5 Osteogenetic differentiation of BMSCs in different extractions. ALP activity was measured using colorimetrically quantitative analysis at 520 nm (A). The expression of osteogenetic marker genes ALP (B), Runx 2 (C), OCN (D) and Col I (E) in cells cultured in different extractions after 14 d were calculated by real time-PCR analysis (* $p < 0.05$, ** $p < 0.01$, compared with the other groups).

3.5. In vivo study

3.5.1. Biomechanical tests

The general observation for the testing groups implanted with different scaffolds at 8 and 16 w are shown in Fig. S2 (ESI[†]). It can be seen that enhanced bone tissue regeneration is achieved for the rhBMP-2 loaded MBG/CPC scaffold compared with that for the others at 8 w, and good osteointegration is obtained in all cases after 16 w of regeneration.

Fig. 6 displays the compression strength of the specimens including different scaffolds. After 8 w, the maximum load for rhBMP-2 loaded MBG/CPC scaffold is 1026 ± 51 N, which is similar to that of the normal group, 1180 ± 34 N. In contrast, the groups of CPC and MBG/CPC scaffolds present the loading values of 811 ± 37 N and 878 ± 28 N, respectively, demonstrating the better effect of rhBMP-2 loaded MBG/CPC scaffold on the repair of bone segment defects. Different from the results mentioned above, the compression strength of all experiment groups show similar loading values to that of the normal group, around 1230 ± 28 N, after 16 w. The corresponding maximum loads are 1093 ± 46 N for the CPC scaffold, 1116 ± 70 N for the MBG/CPC scaffold and 1185 ± 54 N for the rhBMP-2 loaded MBG/CPC scaffold, respectively. These clearly state that the process of osteointegration has been completed for all types of scaffolds after 16 w of regeneration.

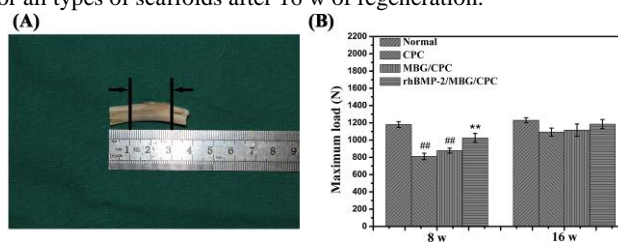


Fig. 6 (A) Image of specimen used for compressive tests (as shown by the arrows). (B) Compressive strength for the specimens including different scaffolds (** $p < 0.01$, compared with the other groups; ## $p < 0.01$, compared with the normal group).

3.5.2. Micro-CT evaluation

Micro-CT images of the bone regeneration in defect sites and reconstructed 3D images of implanted scaffolds are presented in Fig. 7. After 8 w of implantation, bone tissue regeneration can be found for the three testing groups, among which the best new bone formation and the highest degradation of materials are found in the group of rhBMP-2 loaded MBG/CPC scaffold, while incomplete bone defect healing is observed for the control group. With the implantation period extended to 16 w, similar results that all the groups present excellent osteogenetic performance except the control group were obtained. However, least residual materials were observed in the rhBMP-2 loaded MBG/CPC scaffold, demonstrating its improved osteogenetic efficiency and better biodegradability.

3.5.3. Quality and quantity of new bone formation

Fluorescent double-labeling method was employed to detect the rate of new bone formation and mineralization for different scaffolds and the results are shown in Fig. 8. In the first 8 w, the rhBMP-2 loaded MBG/CPC scaffold presents the fastest rate for new bone formation

than that of the CPC and MBG/CPC scaffolds. At 16 w, there is no distinct difference detected among the three groups. Therefore, it is concluded that the rhBMP-2 loaded MBG/CPC scaffold possesses the highest osteogenic capability among the three groups, especially in the initial stage, and the osteogenic ability of the MBG/CPC scaffold is equal to that of the CPC scaffold.

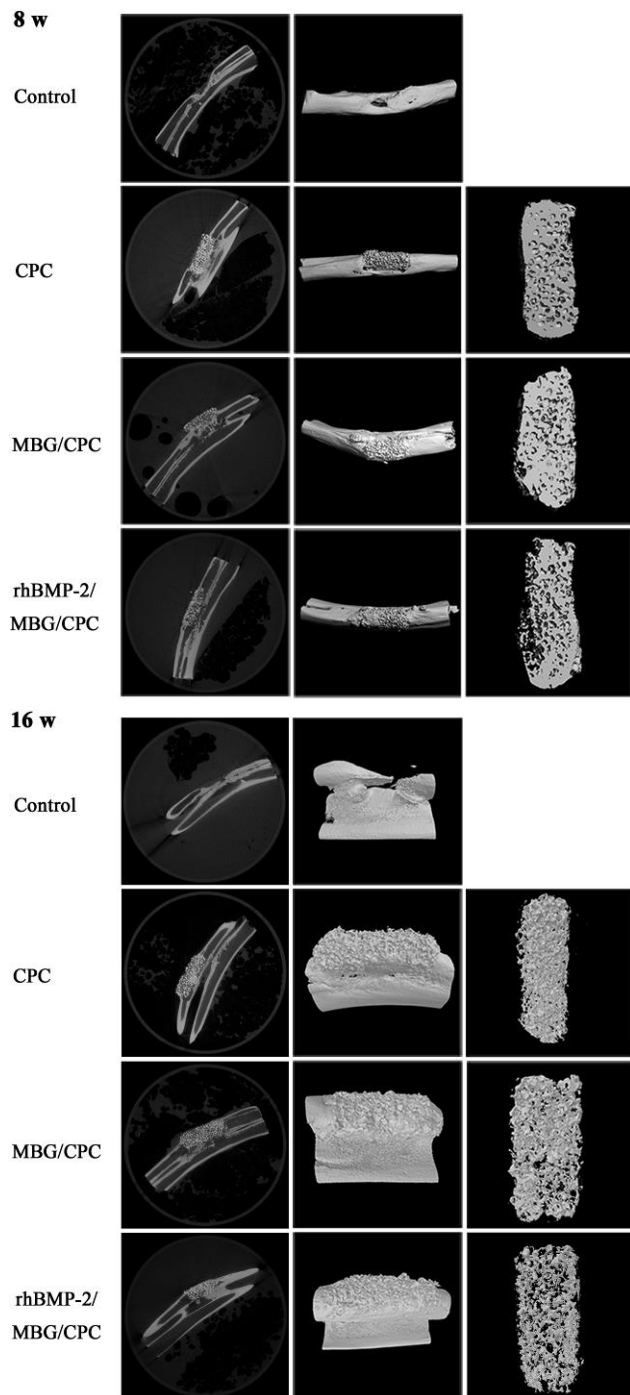


Fig. 7 Micro-CT images (left) of the bone regeneration in the defects and tridimensional reconstruction images of the defect sites (middle) and scaffolds (right).

H&E staining analysis was performed to observe the structure and morphology of bone tissue and the degradation behaviors of different implanting materials. As shown in Fig. S3 (ESI[†]), it reveals

that bone islands are similar both peripherally and centrally within the scaffolds for the three testing groups after 8 w of implantation, suggesting that the bone tissue regeneration has been achieved to a certain extent. Notably, the group of rhBMP-2 loaded MBG/CPC scaffold presents more new bone areas than the others. After 16 w of implantation, bone islands in all of the groups become substantial and compact, and the rhBMP-2 loaded MBG/CPC scaffold shows the best degradation of materials among the three testing groups.

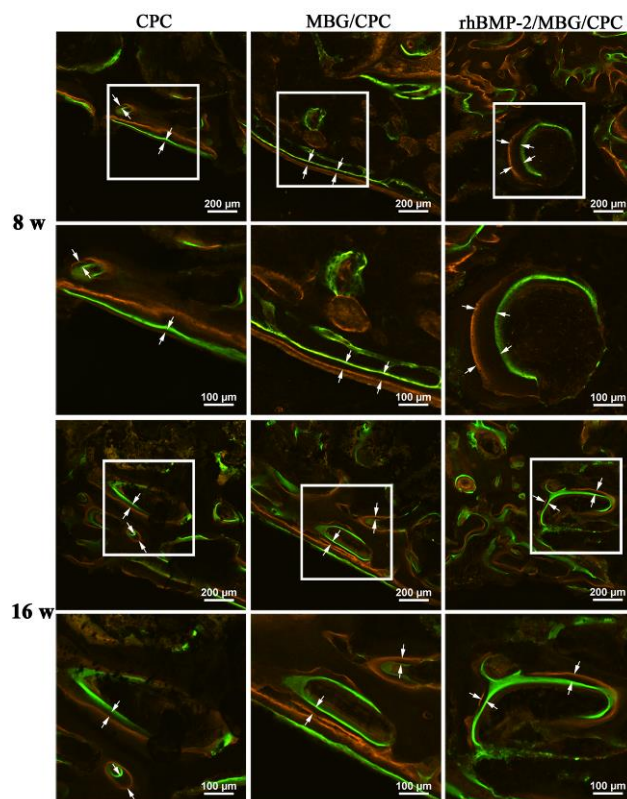


Fig. 8 Fluorescent double-labeling method was employed to detect the growth of new bone tissue. Green and red represent the labeling by Calcein and Alizarin Red S, respectively (The images were taken at 50× magnification). Partial enlarged drawings of the white rectangle areas are displayed in the lower panel (100×). The distance between green lines and red lines (as shown by the arrows) represents the osteogenic ability.

Histological stained sections by Van Gieson's picro fuchsin staining are presented in Fig. 9A. At 8 w, it is clearly found that newly formed bone tissues are distributed around the materials. Compared with the CPC and MBG/CPC scaffolds, the rhBMP-2 loaded MBG/CPC scaffold shows more osteoid depositions on the surface of materials, exhibiting better osteogenic effect. As expected, enhanced osteointegration was achieved for each scaffold at 16 w. Moreover, the degradation of materials can be observed in all testing groups, further demonstrating the results obtained above, where the rhBMP-2 loaded MBG/CPC scaffold holds better biodegradability than the others. Quantification analysis results of the mineralized areas in defects are presented in Fig. 9B. It reveals that the rhBMP-2 loaded MBG/CPC scaffold shows the highest percentage of new bone formation ($20.78 \pm 0.96\%$) at 8 w, followed by the MBG/CPC scaffold ($13.37 \pm 2.48\%$) and the CPC scaffold

(12.96 ± 2.38%). At 16 w, a significantly increased mineralized area was observed for the rhBMP-2 loaded MBG/CPC scaffold, which was calculated to be 25.45 ± 1.78%.

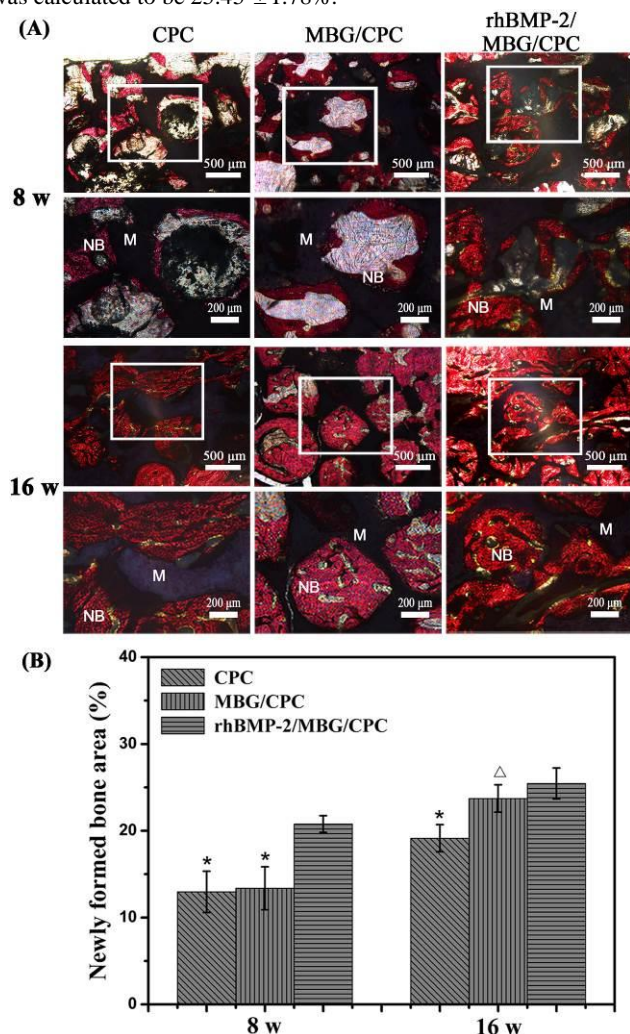


Fig. 9 (A) Histological observations of newly formed bone tissue within different porous scaffolds (V&G staining, the images were taken at 50× magnification). Partial magnifications of the white rectangle areas are displayed in the lower panel (100×, NB: newly formed bone, M: materials). (B) Quantitative analysis of the new bone area after 8 and 16 w of surgery by histological observation (* $p < 0.05$ compared with the rhBMP-2 loaded MBG/CPC group, $\Delta p < 0.05$, the MBG/CPC group vs. the CPC group).

It is well known that osteoinductivity and biodegradability of the implanted biomaterials are of great importance in clinical applications, which can provide favorable conditions for bone tissue regeneration and the feasibility of being gradually replaced by newly formed bone tissue. When the rhBMP-2 loaded MBG/CPC scaffold, which has shown strong osteoinductivity, is introduced into defect sites, the recruitment of native osteoprogenitor cells is accelerated, the differentiation of original cells and fresh cells is promoted, and the subsequent new bone tissue formation are facilitated.⁴¹⁻⁴³ Moreover, the proliferation and differentiation of relative cells will alter the microenvironment around the defects, including pH value and the concentration of ions, which might affect the biodegradation of implant materials.³³ Therefore, it is concluded that the rhBMP-2 loaded MBG/CPC scaffold presents the best combination of

osteoinductivity and biodegradability among all the testing groups, leading to a faster osteointegration process.

4. Conclusions

In summary, a biodegradable rhBMP-2 loaded MBG/CPC scaffold with hierarchical porosity and excellent compressive strength has been successfully fabricated via a simple centrifugal embedding approach and freeze-drying process. It is demonstrated that the incorporation of MBG into CPC scaffold favors the sustained release of rhBMP-2. More importantly, the rhBMP-2 loaded MBG/CPC scaffold presented significantly enhanced osteointegration effect, especially in the initial stage on bone tissue regeneration, in comparison with the CPC and MBG/CPC scaffolds. Furthermore, the rhBMP-2 loaded MBG/CPC scaffold exhibited the best biodegradation of the implanted materials. These suggest that the rhBMP-2 loaded MBG/CPC scaffold is a promising candidate for rapid bone tissue regeneration.

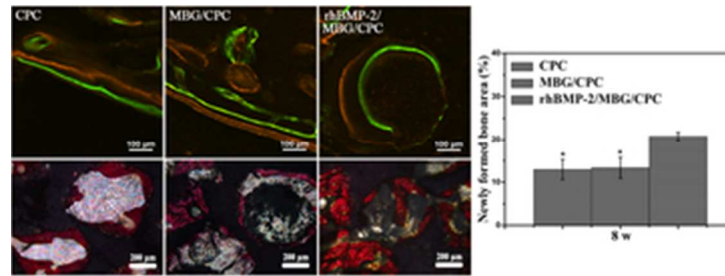
Acknowledgements

This work was supported by the National Basic Research Program of China (2011CB013300, 2012CB933602), the National Natural Science Foundation of China (51172070, 51132009, 51202068, 51472085, 81171707), the Fund for Key Disciplines of Shanghai Municipal Education Commission (2013ZYJB0501), Shu Guang project (11SG30) and the Fundamental Research Funds for the Central Universities.

Notes and references

- 1 I. Drosse, E. Volkmer, S. Seitz, H. Seitz, R. Penzkofer, K. Zahn, U. Matis, W. Mutschler, P. Augat and M. Schieker, *Tissue Eng. Part C*, 2008, **14**, 79.
- 2 B. Fuchs, C. Ossendorf, T. Leerapun and F. H. Sim, *Eur. J. Surg. Oncol.*, 2008, **34**, 1271.
- 3 L. L. Hench, I. D. Xynos and J. M. Polak, *J. Biomater. Sci. Polym. Ed.*, 2004, **15**, 543.
- 4 M. S. Kang, J. H. Kim, R. K. Singh, J. H. Jang and H. W. Kim, *Acta Biomater.*, 2015, **16**, 103.
- 5 K. D. Patel, A. El-Fiqi, H. Y. Lee, R. K. Singh, D. A. Kim, H. H. Lee and H. W. Kim, *J. Mater. Chem.*, 2012, **22**, 24945.
- 6 R. K. Singh, G. Z. Jin, C. Mahapatra, K. D. Patel, W. Chrzanowski and H. W. Kim, *ACS Appl. Mater. Interfaces*, 2015, **7**, 8088.
- 7 K. L. Lin, L. G. Xia, J. B. Gan, Z. Y. Zhang, H. Chen, X. Q. Jiang and J. Chang, *ACS Appl. Mater. Interfaces*, 2013, **5**, 8008.
- 8 H. Li, K. Xue, N. Kong, K. Liu and J. Chang, *Biomaterials*, 2014, **35**, 3803.
- 9 L. Comuzzi, E. Ooms and J. A. Jansen, *Clin. Oral Impl. Res.*, 2002, **13**, 304.
- 10 E. M. Ooms, J. G. C. Wolke, M. T. van de Heuvel, B. Jeschke and J. A. Jansen, *Biomaterials*, 2003, **24**, 989.
- 11 W. J. E. M. Habraken, J. G. C. Wolke and J. A. Jansen, *Adv. Drug Deliv. Rev.*, 2007, **59**, 234.
- 12 G. S. Lee, J. H. Park, U. S. Shin and H. W. Kim, *Acta Biomater.*, 2011, **7**, 3178.
- 13 R. P. Felix Lanao, S. C. G. Leeuwenburgh, J. G. C. Wolke and J. A. Jansen, *Biomaterials*, 2011, **32**, 8839.
- 14 R. Kruger and J. Groll, *Biomaterials*, 2012, **33**, 5887.

- 15 R. A. Perez, K. D. Patel and H. W. Kim, *RSC Adv.*, 2015, **5**, 13411.
- 16 X. X. Yan, C. Z. Yu, X. F. Zhou, J. W. Tang and D. Y. Zhao, *Angew. Chem. Int. Ed.*, 2004, **43**, 5980.
- 17 X. X. Yan, X. H. Huang, C. Z. Yu, H. X. Deng, Y. Wang, Z. D. Zhang, S. Z. Qiao, G. Q. Lu and D. Y. Zhao, *Biomaterials*, 2006, **27**, 3396.
- 18 W. Xia and J. Chang, *J. Control. Release*, 2006, **110**, 522.
- 19 H. S. Yun, S. E. Kim and Y. T. Hyeon, *Chem. Commun.*, 2007, 2139.
- 20 X. Li, X. P. Wang, H. R. Chen, P. Jiang, X. P. Dong and J. L. Shi, *Chem. Mater.*, 2007, **19**, 4322.
- 21 C. T. Wu, W. Fan, Y. F. Zhu, M. Gelinsky, J. Chang, G. Cuniberti, V. Albrecht, T. Friis and Y. Xiao, *Acta Biomater.*, 2011, **7**, 3563.
- 22 M. Zhu, L. X. Zhang, Q. J. He, J. J. Zhao, L. M. Guo and J. L. Shi, *J. Mater. Chem.*, 2011, **21**, 1064.
- 23 C. T. Wu, Y. F. Zhang, Y. F. Zhu, T. Friis and Y. Xiao, *Biomaterials*, 2010, **31**, 3429.
- 24 L. Yu, Y. Li, K. Zhao, Y. F. Tang, Z. Cheng, J. Chen, Y. Zang, J. W. Wu, L. Kong, S. Liu, W. Lei and Z. X. Wu, *PLoS ONE*, 2013, **8**, e62570.
- 25 A. Sadiasa, S. K. Sarkar, R. A. Franco, Y. K. Min and B. T. Lee, *J. Biomater. Appl.*, 2014, **28**, 739.
- 26 A. El-Fiqi, J. H. Kim, R. A. Perez and H. W. Kim, *J. Mater. Chem. B*, 2015, **3**, 1321.
- 27 A. C. M. Renno, F. C. J. van de Watering, M. R. Nejadnik, M. C. Crovace, E. D. Zanotto, J. G. C. Wolke, J. A. Jansen and J. J. P. van den Beucken, *Acta Biomater.*, 2013, **9**, 5728.
- 28 A. C. M. Renno, M. R. Nejadnik, F. C. J. van de Watering, M. C. Crovace, E. D. Zanotto, J. P. M. Hoefnagels, J. G. C. Wolke, J. A. Jansen and J. J. P. van den Beucken, *J. Biomed. Mater. Res. A*, 2013, **101A**, 2365.
- 29 S. K. Lan Levensgood, S. J. Polak, M. J. Poellmann, D. J. Hoelzle, A. J. Maki, S. G. Clark, M. B. Wheeler and A. J. Wagoner Johnson, *Acta Biomater.*, 2010, **6**, 3283.
- 30 J. M. Wozney and V. Rosen, *Clin. Orthop. Relat. Res.*, 1998, **346**, 26.
- 31 W. K. Hsu, O. Sugiyama, S. H. Park, A. Conduah, B. T. Feeley, N. Q. Liu, L. Krenek, M. S. Virk, D. S. An, I. S. Chen and J. R. Lieberman, *Bone*, 2007, **40**, 931.
- 32 X. Q. Jiang, J. Zhao, S. Y. Wang, X. J. Sun, X. L. Zhang, J. Chen, D. L. Kaplan and Z. Y. Zhang, *Biomaterials*, 2009, **30**, 4522.
- 33 J. Zhang, H. J. Zhou, K. Yang, Y. Yuan and C. S. Liu, *Biomaterials*, 2013, **34**, 9381.
- 34 T. Kokubo and H. Takadama, *Biomaterials*, 2006, **27**, 2907.
- 35 J. J. Cao, B. R. Gregoire and H. Gao, *Bone*, 2009, **44**, 1097.
- 36 Y. F. Zhang, C. T. Wu, T. Friis and Y. Xiao, *Biomaterials*, 2010, **31**, 2848.
- 37 W. J. Zhang, G. C. Wang, Y. Liu, X. B. Zhao, D. H. Zou, C. Zhu, Y. Q. Jin, Q. F. Huang, J. Sun, X. Y. Liu, X. Q. Jiang and H. Zreiqat, *Biomaterials*, 2013, **34**, 3184.
- 38 X. F. Niu, Q. L. Feng, M. B. Wang, X. D. Guo and Q. X. Zheng, *J. Control. Release*, 2009, **134**, 111.
- 39 B. Li, T. Yoshii, A. E. Hafeman, J. S. Nyman, J. C. Wenke and S. A. Guelcher, *Biomaterials*, 2009, **30**, 6768.
- 40 J. P. M. Issa, M. V. L. B. Bentley, M. M. Iyomasa, W. Sebald and R. F. De Albuquerque, *Anat. Histol. Embryol.*, 2008, **37**, 181.
- 41 C. T. Wu, Y. F. Zhang, X. B. Ke, Y. X. Xie, H. Y. Zhu, R. Crawford and Y. Xiao, *J. Biomed. Mater. Res. A*, 2010, **95A**, 476.
- 42 C. L. Dai, H. Guo, J. X. Lu, J. L. Shi, J. Wei and C. S. Liu, *Biomaterials*, 2011, **32**, 8506.
- 43 J. H. Bae, H. R. Song, H. J. Kim, H. C. Lim, J. H. Park, Y. C. Liu and S. H. Teoh, *Tissue Eng. Part A*, 2011, **17**, 2389.



RhBMP-2/MBG/CPC scaffold is beneficial for rapid bone tissue regeneration in the early stage.
30x11mm (300 x 300 DPI)